Quantitative Study of Articular Cartilage Based on Greyscale Assessment Using Low-Field MRI

Rizwana Seeni Ibramsa[a,*], Mohd Juzaila Abd Latif[a,b], Mohamad Shukri Zakaria[a], Muhamad Noor Harun[c], Jamaluddin Mahmud[d]

[a] Fakulti Kejuruteraan Mekanikal, Universiti Teknikal Malaysia Melaka, Hang Tuah Jaya 76100 Durian Tunggal, Melaka, Malaysia
[b] Advanced Manufacturing Centre (AMC), Universiti Teknikal Malaysia Melaka, Hang Tuah Jaya 76100 Durian Tunggal, Melaka, Malaysia
[c] Faculty of Engineering, Universiti Teknologi Malaysia, 81310 Skudai, Johor, Malaysia
[d] Faculty of Mechanical Engineering, Universiti Teknologi MARA, 40450 Shah Alam, Selangor, Malaysia
Corresponding author: *wana.max88@gmail.com

Abstract— Osteoarthritis is a degenerative disorder that changes the biomechanical properties of articular cartilage in its development phase. MRI has become the diagnosing tool used widely to examine the articular cartilage in the synovial joint since it can provide excellent soft-tissue contrast. However, most diagnoses were conducted using clinical high-field MRI, while the low-field MRI was only used to obtain the geometrical data. This study aims to quantitatively assess the biomechanical properties of cartilage tissue using a low-field MRI system based on the image greyscale assessment. The articular cartilage image of intact bovine hip joints was obtained using 0.18 T MRI. The MRI images were characterized based on the intensity of the greyscale. The biomechanical properties of elastic modulus and permeability of cartilage were subsequently characterized by incorporating the creep indentation test data with the computational finite element model. Further correlation analyses were performed to examine the relationship between the greyscale of MRI images and biomechanical properties of elastic modulus and permeability of the cartilage. The cartilage greyscale was found to be strongly associated with the cartilage biphasic elastic modulus ($r = 0.85$), while the permeability ($r = -0.51$) was observed to have a moderate correlation with the greyscale. These findings show the capability of low-field MRI to produce an image that correlates with the articular cartilage's biomechanical properties, which could be adapted as a biomarker to detect osteoarthritis earlier than usual.

Keywords— Articular cartilage; low-field MRI; elastic modulus; greyscale; permeability.

I. INTRODUCTION

Osteoarthritis is a common joint disease that limits human movement and affects daily life activities. It is most prevalent in the knee, hip, and spine, leading to chronic joint pain [1], [2]. In 2015, the World Health Organization reported that 9.6% of men and 18 % of women above 60 years old had been affected by symptomatic osteoarthritis. As the aging population of the developed country increases, the prevalence of osteoarthritis is expected to accelerate from 2015 to 2050 due to the substantial increase of the world's population over 60 years old [3], [4].

It is well recognized that the main cause of osteoarthritis is the deterioration of articular cartilage in a synovial joint. The progression of the degenerating characteristics affects the biomechanical properties of the articular cartilage from the early stage of osteoarthritis [5], [6]. This is due to the hydration of cartilage, where the tissue becomes porous and highly permeable, decreasing the modulus of elasticity and load-bearing capacity [7], [8].

Since the cartilage tissue has limited regenerative capability, tissues repair remains a challenging task.

The cartilage tissue can be categorized as biphasic material with distinct fluid and solid phases. It consists of 65 to 80% water, while the solid phase is mainly from an extracellular matrix composed of collagens and proteoglycans [9], [10]. The concentration of water content, proteoglycan and collagen fibrils varies throughout the depth of the cartilage tissue to restrain the macromolecular environment within the tissue [7], [8]. The degeneration of the macromolecular constituents in articular cartilage affects the mechanical properties of the tissue.

The most successful non-invasive diagnosis of joint disease and clinical imaging has been magnetic resonance imaging (MRI), particularly for cartilage injury detection.

This is due to its working principle and the content of cartilage tissue [6], [11]. MRI can be categorized based on the magnetic strength as low-field MRI (0.1-0.5 T), mid-field MRI (0.5-1.5 T), high-field MRI (1.5-3 T), very high-field MRI (4-7 T), and ultra-high-field MRI (> 7 T). Most of the earlier cartilage research were performed utilizing either mid-field or high-field MRI systems, with limited research specifically contrasting the accuracy of various high-field and low-field MRI systems in joint condition diagnostics [12], [13]. However, low-field MRI has shown the potential of producing similar image quality of high-field MRI [14], [15].

The low-field MRI systems were only used in previous studies to determine articular cartilage morphology to assess the loss of thickness and volume [16], [17]. The ability of low-field MRI to evaluate the condition of cartilage tissue has not been fully explored in previous studies. In the early detection of osteoarthritis, it is important to monitor the biomechanical properties of the cartilage and examine physiological changes of the tissue. Furthermore, the correlation of the quantitative low-field MRI image greyscale and cartilage biomechanical properties of elastic modulus and permeability is not fully explored. Therefore, the purpose of this study is to evaluate the potential of a low-field MRI system to examine the cartilage tissue based on a greyscale assessment of the image. The outcome of this study could be used as a preventive strategy to increase the effectiveness of detecting degenerated articular cartilage at an early stage using low-field MRI.

II. Material and Methods

A. Specimen Preparation

Bovine hip joints were obtained within 24 hours after slaughter from a local abattoir. Excess flesh and ligaments were discarded using a scalpel, scissors, and an electric handsaw. The intact hip joints (n=6) with both femoral head and acetabulum parts attached were wrapped with a plastic wrapper in moist condition. The fresh joints were stored in a refrigerator with a temperature of 4°C before MRI scanning.

The hip joint was separated once the MRI scan was performed to extract the cartilage specimens from the femoral head for indentation test. The cartilage specimens (n=24) were obtained from four sections of the femoral head which were lateral left (LL), medial left (ML), lateral right (LR), and medial right (MR) as shown in Fig. 1.
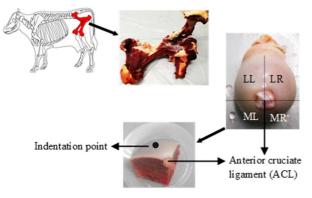

Fig. 1 Bovine hip joint specimen

An anterior cruciate ligament (ACL) was made as to the reference point because it was identified in the MRI scanning
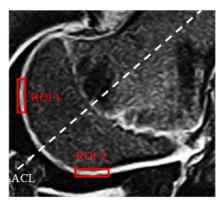
images. Phosphate-buffered saline (PBS) was applied to the cartilage surface to keep the tissue hydrated throughout the process.

B. Low-field Magnetic Resonance Imaging

The intact hip joints were scanned using 0.18 T Esaote C-scan (Genova, Italy) MRI system that generated 0 to 4,096 grey values. Five imaging sequences, which were previously used in low-field MRI systems, were applied to scan the intact hip joint [17], [18]. This is to determine the sequence that could produce a clear image of the cartilage. The imaging sequences were the gradient-echo (GE), gradient-echo short-T1 inversion recovery (GE-STIR), spin-echo T1 (SE-T1), spin-echo T2 (SE-T2), and turbo spin-echo (Turbo SE). The parameters of the imaging sequences are tabulated in Table 1.

TABLE I
IMAGING PARAMETERS OF LOW-FIELD MRI FOR DIFFERENT SEQUENCES

Parameters	Sequences				
	GE	GE STIR	SE T1	SE T2	Turbo SE
Echo time (ms)	18	16	26	90	90
Repetition time (ms)	2660	2400	2900	4940	4940
No. of slices	59	59	59	59	59
Field of view (mm)	180	180	180	180	180
Matrix	256	256	256	256	256
Thickness (mm)	2	2	2	2	2

The imaging sequence was visually assessed on the quality of the cartilage image. Further assessment of the sequence was carried out to evaluate the generated greyscale range using Student-t test (p<0.05) [18], [19].

C. MRI Image Assessment

The MRI images were stored in standard Digital Imaging and Communication in Medicine (DICOM) image format and processed using Matlab software (R2019b, MathWorks Inc., MA, USA). The cartilage image was characterized based on the greyscale intensity of every pixel in the region of interest (ROI), as shown in Fig. 2. The ROI locations were selected at the identified points to perform the indentation test.

Fig. 2 Low-field MRI image of bovine hip joint with identified ROIs

D. Characterization of Biomechanical Properties

The biphasic biomechanical properties of elastic modulus and permeability were characterized using a combination of creep indentation test and finite element (FE) analysis [20]. The cartilage specimen was indented at the ROI using 4 mm diameter spherical indenter using the indentation test set-up as shown in Fig. 3. The test was subjected to 0.38 N compression load, which resulted between 10% to 20% deformation of the cartilage thickness. Cartilage displacement was recorded using LabVIEW data acquisition software (National Instruments Corporation, Austin, TX, USA) every 0.01 seconds for at least 2000 seconds so that the cartilage deformation reached at equilibrium state. During the test, the cartilage specimen was submerged in PBS to avoid the tissue from dehydrated.
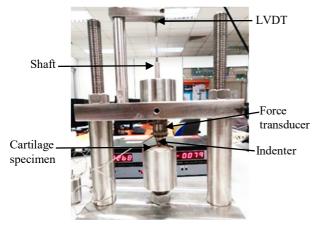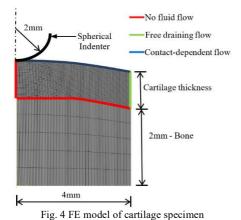

Fig. 3 Creep indentation test set-up

The cartilage thickness was then measured using a sharp needle indenter assembled to the shaft of indentation test apparatus. Indentation load of 3.16 N was applied to penetrate the cartilage tissue until it reached the underlying subchondral bone. The displacement of the needle indenter and the load were recorded every 0.001 seconds to obtain accurate measurement of the cartilage thickness. As previously stated, the thickness was determined based on the needle position at the cartilage surface and subchondral bone [20].

The articular cartilage was modelled as axisymmetric biphasic poroelastic element to represent the solid and fluid phases of the tissue using Abaqus 6.14 (DS Simulia Corp., Providence, RI, USA) software. The FE model of the cartilage was developed using the measured thickness with 4 mm width and the subchondral bone as shown in Fig. 4.

Fig. 4 FE model of cartilage specimen

Meanwhile, the 2 mm radius spherical indenter was modelled as analytical rigid surface. The cartilage was modelled using four-node bilinear displacement and pore pressure (CAX4P) elements, while the subchondral bone was represented using four-node bilinear (CAX4) elements with the elastic modulus of 2000 MPa and a Poisson's ratio of 0.2 [20].

In terms of boundary condition, the nodes along the axisymmetric axis were restricted in horizontal direction, while the movement in horizontal and vertical directions was restricted at the bone's base nodes. The movement of spherical indenter was constrained to actuate in vertical direction. Contact-dependent flow was applied at the top of the cartilage surface [20]. In addition, fluid flow was prevented at the bottom and the vertical symmetry axis of cartilage surface. For the outer edge of the cartilage, the nodes were maintained at zero pore pressure to allow the unrestricted fluid flow. These boundary and interface conditions were applied to simulate the experimental creep indentation test.

The FE model was consequently incorporated with the creep indentation test data to characterize the biomechanical properties of the cartilage. The elastic modulus and permeability values were iteratively changed in the FE model to match the experiment deformation-time curve using the non-linear least-squares method in MATLAB software (R2019, MathWorks Inc., MA, USA). The optimized properties were obtained when the function reached the minimum squared error between the curves [20].

E. Correlation of Biomechanical Properties and MRI Image

Linear Pearson correlation coefficient was imposed to determine the relationship between the greyscale of MRI image and the biomechanical properties of the cartilage. The linear correlation coefficient, r was used to measure the strength of the linear relationship between the image greyscale and biomechanical properties.
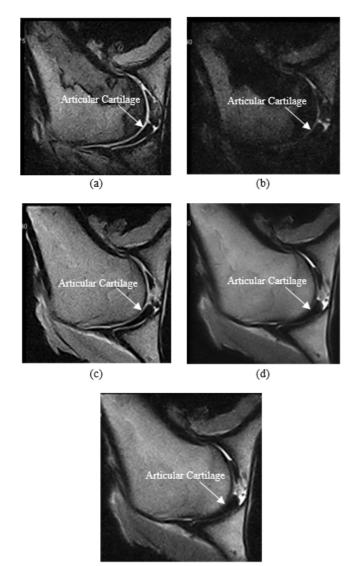
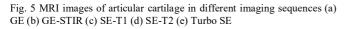## III. RESULTS AND DISCUSSION

A. Evaluation of Low-field MRI Sequence

Five imaging sequences utilized in previous low-field MRI studies were assessed to obtain the best sequence that can produce clear image of articular cartilage prior further image analysis. The sequences include gradient echo (GE), gradient echo short-T1 inversion recovery (GE-STIR), spin echo T1 (SE-T1), spin echo T2 (SE-T2) and turbo spin echo (Turbo SE). As expected, different qualities of cartilage images were produced as shown in Fig. 5.

It was observed that the GE and SE-T1 imaging sequences showed clear and better image quality with good contrast between articular cartilage and the surrounding tissues compared to other sequences. These imaging sequences were also used in previous studies using other low-field MRI systems to generate articular cartilage image to examine the morphology of articular cartilage such as cartilage thickness, volume, and joint space [16]–[18]. This is due to the better definition of the anatomic structure of the synovial joint that maximizes the signal and contrast between the joint structures.

Fig. 5 MRI images of articular cartilage in different imaging sequences (a) GE (b) GE-STIR (c) SE-T1 (d) SE-T2 (e) Turbo SE

The range of grayscale for the articular cartilage produced from the GE and SE-T1 imaging sequences were then analyzed to evaluate the statistical significance using statistical t-test analysis. The greyscale generated from the GE imaging sequence was found to be statistically significant (p < 0.05) compared to SE-T1 imaging sequence. Therefore, based on the greyscale's image quality and statistical analysis, the GE imaging sequence was noted to be the most reliable imaging sequence to assess the articular cartilage using the low-field MRI system. Previous studies have also shown that at low-field strength, signal-to-noise ratio (SNR) and contrast-to-noise ratio (CNR) of GE is better compared with SE sequence to give better visualization of cartilage tissue and better contrast between cartilage and both synovial fluid and the subchondral bone plate [18], [21].

B. Greyscale Intensity of Articular Cartilage

This study obtained two layers of pixel throughout the cartilage thickness from the MRI images due to the plane resolution of 0.70 mm for each pixel. These two layers can be categorized as superficial zone and deep zone of the cartilage.

Previous studies also found the cartilage with two pixel layers in the analysis of depth and angle dependence using low-field MRI [22], [23]. Therefore, differences in the average greyscale between the layers were observed through the entire thickness of the articular cartilage. Fig. 6 shows the average greyscale of the superficial zone was 1340.30 ± 373.41, while the deep zone was 1220.43 ± 422.90. The greyscale of the superficial zone was 9.36% higher than the deep zone. This is also in agreement with previous findings where the highest water content was found at the superficial zone of the cartilage [24], [25].
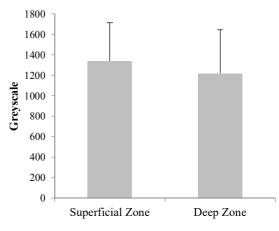

Fig. 6 Average greyscale of the superficial and deep zones

Apart from its water content, the collagens in cartilage tissue produce localized differences MRI transverse relaxation time (T2) value. Xia et al. [22] have described the T2 varied with depth of the articular surface due to collagen fibril orientation on the external magnetic field. The T2 anisotropy has a strong influence on the MRI images of articular cartilage. In another study by Watrin et al. [26], the T2 anisotropy value was also observed higher at the superficial layer compared to the deeper layer of the cartilage. These coincide with the present study that the differences in greyscale values attributed to the depth-related variation in the cartilage composition throughout the entire thickness of the articular layer. It indicates that various physiological characteristics within the thickness of the articular cartilage could be examined using the image greyscale of low-field MRI.

C. Biomechanical Properties of Articular Cartilage

Based on the present result, the characterized elastic modulus and permeability showed topographical variation across the articular cartilage of the bovine femoral head as shown in Fig. 7. Distinctive variation of biomechanical properties was observed where the tissue at right side was stiffer and more permeable as compared to the left side of the femoral head. The variation indicates the irregular physiological loading and functional requirements across the articular cartilage of the femoral head in hip joint. This was also found in previous studies [27]. The average values of elastic modulus and permeability were 1.70 ± 0.65 MPa and $0.53 \pm 0.25 \times 10^{-15}$ m^4/Ns respectively, which was within the range compared with previous reported values for bovine femoral head [28], [29].
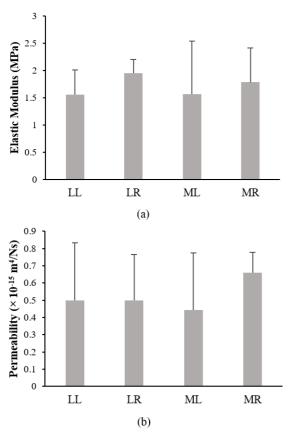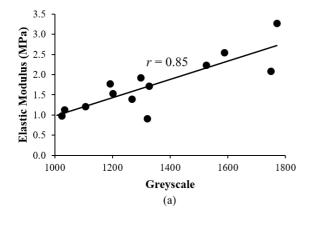
Fig. 7 Biomechanical properties at four distinct quadrants of femoral head (a) Elastic modulus (b) Permeability

D. Correlation of Biomechanical Properties and Greyscale of Cartilage

Linear Pearson correlation analysis was used to evaluate the relationship between the low-field MRI image and the biomechanical properties of the cartilage. The cartilage greyscale was found to be strongly associated with the cartilage biphasic elastic modulus ($r = 0.85$). However, opposite trend with moderate correlation ($r = -0.51$) was observed between the permeability and greyscale value where the permeability decreased as the greyscale value increased as shown in Fig. 8. This is mainly due to higher water content in the cartilage that reduced the permeability and produced brighter MRI image. These relationship trends were also found between quantitative MRI imaging parameters and cartilage biomechanical properties using high-field and ultra-high-field MRI systems [29], [30].
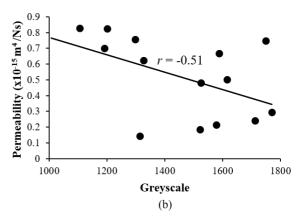

(a)

(b)

Fig. 8 Linear Pearson correlation of cartilage greyscale and biomechanical properties (a) Elastic modulus (b) Permeability

The intrinsic biomechanical properties of cartilage have been shown to be related to its extracellular matrix particularly collagen and proteoglycan [9], [31]. Previous studies have also investigated the relationship between quantitative MRI imaging parameters and cartilage biomechanical properties using high-field and ultra-high-field MRI systems [6], [30]. However, Lammentausta *et al.* [32] have observed statistical linear correlation between T2 and elastic modulus using 1.5 T and 9.4 T MRI which the field strength did not affect the topographical variation of the T2 that was similar to the elastic modulus of cartilage. In addition, the T2 anisotropy was closely associated with the collagen framework in the magnetic field and it has been found that collagen content was a great determinant of MRI signal intensity [22], [26], [33]. These outcomes could provide a significant parameters of quantitative MRI measurements for articular cartilage using low-field MRI.

IV. CONCLUSIONS

In the present study, the low-field MRI have the capacity to produce quality image of articular cartilage. The range of the generated greyscale value of the cartilage can be assessed throughout the thickness which could be used for further analysis. Based on the results, the low-field MRI has the potential to conduct quantitative measurement where promising correlations were observed between the MRI image greyscale and biomechanical properties of the cartilage. It could be used as a preventive strategy to increase the effectiveness to detect the degenerated articular cartilage at early stage using low-field MRI.

NOMENCLATURE

E	elastic modulus	MPa
r	linear correlation coefficient	

Greek letters

κ	permeability	m⁴/Ns

REFERENCES

[1] T. W. O'Neill, P. S. McCabe, and J. McBeth, "Update on the Epidemiology, Risk Factors and Disease Outcomes of Osteoarthritis," *Best Pract. Res. Clin. Rheumatol.*, vol. 32, no. 2, pp. 312–326, 2018.

[2] N. Walsh, L. Jones, S. Phillips, R. Thomas, L. Odondi, S. Palmer, F. Cramp, J. Pollock and M. Hurley, "Facilitating Activity and Self-Management for People with Arthritic Knee, Hip or Lower Back Pain (FASA): A Cluster Randomised Controlled Trial," *Musculoskelet. Sci. Pract.*, vol. 50, no. 1, pp. 102271(1)-102271(7), 2020.

[3] A. Postler, A. L. Ramos, J. Goronzy, K.-P. Gunther, T. Lange, J. Schmitt, A. Zink and F. Hoffmann, "Prevalence and Treatment of Hip and Knee Osteoarthritis in People Aged 60 Years or Older in Germany: An Analysis Based on Health Insurance Claims Data," *Clin. Interv. Aging*, vol. 13, pp. 2339–2349, 2018.

[4] D. J. Hunter and S. Bierma-Zeinstra, "Osteoarthritis," *Lancet*, vol. 393, no. 10182, pp. 1745–1759, 2019.

[5] H. C. Cutcliffe and L. E. DeFrate, "Comparison of Cartilage Mechanical Properties Measured During Creep and Recovery," *Sci. Rep.*, vol. 10, no. 1547, pp. 1–8, 2020.

[6] A. T. Collins, C. C. Hatcher, S. Y. Kim, S. N. Ziemian, C. E. Spritzer, F. Guilak, L. E. DeFrate and A. L. McNulty, "Selective Enzymatic Digestion of Proteoglycans and Collagens Alters Cartilage T1rho and T2 Relaxation Times," *Ann. Biomed. Eng.*, vol. 47, no. 1, pp. 190–201, 2019.

[7] M. E. Mononen, P. Tanska, H. Isaksson, and R. K. Korhonen, "New Algorithm for Simulation of Proteoglycan Loss and Collagen Degeneration in the Knee Joint: Data from the Osteoarthritis Initiative," *J. Orthop. Res.*, vol. 36, no. 6, pp. 1673–1683, 2018.

[8] D. Warnecke, J. Balko, J. Haas, R. Bieger, F. Leucht, N. Wolf, N. Schild, S. Stein, A. Seitz, A. Ignatius, H. Reichel, B. Mizaikoff and L. Dürselen, "Degeneration Alters the Biomechanical Properties and Structural Composition of Lateral Human Menisci," *Osteoarthr. Cartil.*, vol. 28, no. 11, pp. 1482–1491, 2020.

[9] T. Hafner, J. Schock, M. Post, D. Abrar, P. Sewerin, K. Linka, M. Knobe, C. Kuhl, D. Truhn and S. Nebelung, 2020., "A Serial Multiparametric Quantitative Magnetic Resonance Imaging Study to Assess Proteoglycan Depletion of Human Articular Cartilage and its Effects on Functionality," *Sci. Rep.*, vol. 10, no. 1, pp. 1–18, 2020.

[10] C. S. Thudium, A. Engstrom, S. S. Groen, M. A. Karsdal, A. C. Bay-Jensen, and N. Bioscience, "An Ex Vivo Tissue Culture Model of Cartilage Remodeling in Bovine Knee Explants," *J. Vis. Exp.*, vol. 2019, no. 153, p. e59467, 2019.

[11] D. Abrar, C. Schleich, S. Nebelung, M. Frenken, T. Ullrich, K. Radke, G. Antoch, S. Vordenbäumen, R. Brinks, M. Schneider, B. Ostendorf and P. Sewerin, "Proteoglycan Loss in the Articular Cartilage is Associated with Severity of Joint Inflammation in Psoriatic Arthritis - A Compositional Magnetic Resonance Imaging Study," *Arthritis Res. Ther.*, vol. 22, no. 124, pp. 1–10, 2020.

[12] Q. Cheng and F.-C. Zhao, "Comparison of 1.5- and 3.0-T Magnetic Resonance Imaging for Evaluating Lesions of the Knee," *Medicine (Baltimore).*, vol. 97, no. 38, p. e12401, 2018.

[13] J. Daglish, D. D. Frisbie, K. T. Selberg, and M. F. Barrett, "High Field Magnetic Resonance Imaging is Comparable with Gross Anatomy for Description of the Normal Appearance of Soft Tissues in the Equine Stifle," *Vet. Radiol. Ultrasound*, vol. 59, no. 6, pp. 721–736, 2018.

[14] H.-M. Klein, "Low-Field Magnetic Resonance Imaging," *RoFo Fortschritte auf dem Gebiet der Rontgenstrahlen und der Bildgeb. Verfahren*, vol. 192, no. 6, pp. 537–548, 2020.

[15] M. Biggi and S. J. Dyson, "Use of High-Field and Low-Field Magnetic Resonance Imaging to Describe the Anatomy of the Proximal Portion of the Tarsal Region of Nonlame Horses," *Am. J. Vet. Res.*, vol. 79, no. 3, pp. 299–310, 2018.

[16] C. van Zadelhoff, T. Schwarz, S. Smith, A. Engerand, and S. Taylor, "Identification of Naturally Occurring Cartilage Damage in the Equine Distal Interphalangeal Joint Using Low-Field Magnetic Resonance Imaging and Magnetic Resonance Arthrography," *Front. Vet. Sci.*, vol. 6, pp. 508(1)-508(10), 2020.

[17] J. Głodek, K. Milewska, A. Tobolska, Ł. Grabarczyk, W. Maksymowicz, I. Bada, I. and Z. Adamiak, "Feline Hip Joint Anatomy in Magnetic Resonance Images," *J. Vet. Med. Ser. C Anat. Histol. Embryol.*, vol. 48, no. 5, pp. 449–454, 2019.

[18] J. Olive, "Distal Interphalangeal Articular Cartilage Assessment using Low-Field Magnetic Resonance Imaging," *Vet. Radiol. Ultrasound*, vol. 51, no. 3, pp. 259–266, 2010.

[19] S. Hangaard, H. Gudbergsen, C. L. Daugaard, H. Bliddal, J. D. Nybing, M. T. Nieminen, V. Casula, C.-J, Tiderius and M. Boesen, "Delayed Gadolinium-Enhanced MRI of Menisci and Cartilage (dGEMRIM/dGEMRIC) in Obese Patients with Knee Osteoarthritis: Cross-Sectional Study of 85 Obese Patients with Intra-Articular Administered Gadolinium Contrast," *J. Magn. Reson. Imaging*, vol. 48, no. 6, pp. 1700–1706, 2018.

[20] N. H. Hashim, M. J. Abd Latif, Y. L. Jaafar, R. Ramlan, and J. Mahmud, "Computational and Experimental Study of Articular Cartilage Thickness on Biomechanical Behavior," *Int. J. Appl. Eng. Res.*, vol. 12, no. 16, pp. 5849–5856, 2017.

[21] M. Encinoso, J. Orós, G. Ramírez, J. R. Jaber, A. Artiles, and A. Arencibia, "Anatomic Study of the Elbow Joint in a Bengal Tiger (Panthera Tigris Tigris) using Magnetic Resonance Imaging and Gross Dissections," *Animals*, vol. 9, no. 12, pp. 1–13, 2019.

[22] Y. Xia, J. B. Moody, N. Burton-Wurster, and G. Lust, "Quantitative in situ Correlation between Microscopic MRI and Polarized Light Microscopy Studies of Articular Cartilage," *Osteoarthr. Cartil.*, vol. 9, no. 5, pp. 393–406, 2001.

[23] T. Nozaki, Y. Kaneko, H. Yu, K. Kaneshiro, R. Schwarzkopf, T. Hara and H. Yoshioka, "T1rho mapping of entire femoral cartilage using depth- and angle-dependent analysis," *Eur. Radiol.*, vol. 26, no. 6, pp. 1952–1962, 2016.

[24] L. Cai, E. A. Nauman, C. B. W. Pedersen, and C. P. Neu, "Finite Deformation Elastography of Articular Cartilage and Biomaterials Based on Imaging and Topology Optimization," *Sci. Rep.*, vol. 10, no. 1, pp. 1–12, 2020.

[25] P. A. Torzilli and A. Azimulla, "Ultraviolet Light (365 nm) Transmission Properties of Articular Cartilage as a Function of Depth, Extracellular matrix, and Swelling," *J. Biomed. Mater. Res. - Part A*, vol. 108, no. 2, pp. 327–339, 2020.

[26] A. Watrin, J. Ruaud, P. Olivier, N. Guingamp, P. Gonord, P. Netter, A. Blum, G. Guillot, P. Gillet and B. Loeuille, "T2 Mapping of Rat Patellar Cartilage," *Radiology*, vol. 219, no. 2, pp. 395–402, 2001.

[27] K. A. Athanasiou, A. Agarwal, A. Muffoletto, F. J. Dzida, G. Constantinides, and M. Glem, "Biomechanical Properties of Hip Cartilage in Experimental Animal Models," *Clin. Orthop. Relat. Res.*, vol. 316, pp. 254–266, 1995.

[28] D. K. Temple, A. A. Cederlund, B. M. Lawless, R. M. Aspden, and D. M. Espino, "Viscoelastic Properties of Human and Bovine Articular Cartilage: A Comparison of Frequency-Dependent Trends," *BMC Musculoskelet. Disord.*, vol. 17, no. 1, pp. 1–8, 2016.

[29] M. T. Nieminen, J. Toyras, M. S. Laasanen, J. Silvennoinen, H. J. Helminen, and J. S. Jurvelin, "Prediction of Biomechanical Properties of Articular Cartilage with Quantitative Magnetic Resonance Imaging," *J. Biomech.*, vol. 37, no. 3, pp. 321–328, 2004.

[30] O. Nykänen, J. Sarin, J. Ketola, H. Leskinen, N. te Moller, V. Tiitu, I. Mancini, J. Visser, H. Brommer, P. van Weeren, J. Malda, J. Töyräs and M. Nissi, "T2* and Quantitative Susceptibility Mapping in an Equine Model of Post-Traumatic Osteoarthritis: Assessment of Mechanical and Structural Properties of Articular Cartilage," *Osteoarthr. Cartil.*, vol. 27, no. 10, pp. 1481–1490, 2019.

[31] M. Danalache, R. Kleinert, J. Schneider, A. Erler, M. Schwitalle, R. Riester, F. Traub and U. Hofmann, "Changes in Stiffness and Biochemical Composition of the Pericellular Matrix as a Function of Spatial Chondrocyte Organisation in Osteoarthritic Cartilage," *Osteoarthr. Cartil.*, vol. 27, no. 5, pp. 823–832, 2019.

[32] E. Lammentausta, P. Kiviranta, M. Nissi, M. Laasanen, I. Kiviranta, M. Nieminen and J. Jurvelin, "T2 Relaxation Time and Delayed Gadolinium-Enhanced MRI of Cartilage (dGEMRIC) of Human Patellar Cartilage at 1.5 T and 9.4 T: Relationships with Tissue Mechanical Properties," *J. Orthop. Res.*, vol. 61, no. February, pp. 254–262, 2006.

[33] M. L. Richardson, B. Amini, and T. L. Richards, "Some New Angles on the Magic Angle: What MSK Radiologists Know and Don't Know about this Phenomenon," *Skeletal Radiol.*, vol. 47, no. 12, pp. 1673–1681, 2018.